The Spectral Energy Distribution of Galaxies
Proceedings IAU Symposium No. 284, 2011
R.J. Tuffs & C.C. Popescu, eds.

doi:10.1017/S1743921312009660

Multi-wavelength probes of distant lensed galaxies

Stephen Serjeant
Dept. of Physical Sciences, The Open University, Milton Keynes, MK7 6AA, UK
email: s.serjeant@open.ac.uk

Abstract. I summarise recent results on multi-wavelength properties of distant lensed galaxies, with a particular focus on *Herschel*. Submm surveys have already resulted in a breakthrough discovery of an extremely efficient selection technique for strong gravitational lenses. Benefitting from the gravitational magnification boost, blind mm-wave redshifts have been demonstrated on IRAM, SMA and GBT, and follow-up emission line detections have been made of water, [OIII], [CII] and other species, revealing the PDR/XDR/CRDR conditions. I also discuss HST imaging of submm lenses, lensed galaxy reconstruction, the prospects for ALMA and e-Merlin and the effects of differential magnification. Many emission line diagnostics are relatively unaffected by differential magnification, but SED-based estimates of bolometric fractions in lensed infrared galaxies are so unreliable as to be useless, unless a lens mass model is available to correct for differential amplification.

Keywords. gravitational lensing, surveys, galaxies: active, galaxies: high-redshift, galaxies: ISM, galaxies: starburst, cosmology: dark matter, infrared: galaxies, radio continuum: galaxies, submillimeter

1. Introduction

Gravitational lens magnification is a fast route to faint object and faint population studies. This technique has been exploited to reveal or constrain the populations responsible for integrated far-IR and submm extragalactic backgrounds (e.g. Smail *et al.* 1997, Knudsen *et al.* 2008). Lensing is also one of the few available means of inferring the distribution of dark matter in galaxies (e.g. Gavazzi *et al.* 2007). Rare lens configurations even have the promise of yielding $\Omega_{\rm M}$ and w to 10%; this requires 50 double Einstein rings, requiring in turn a parent sample of thousands of lenses (Gavazzi *et al.* 2008). Indeed many current and future applications of lensing are limited by sample size (Treu 2010). Furthermore, most lens surveys have selected strongly for foreground lenses at relatively low redshifts, e.g. $z < 0.2$, restricting studies of the evolving dark matter distribution in galaxies. These are strong drivers for both larger and higher redshift samples of lenses.

The past year has seen an explosion of interest in submm-selected strong gravitational lenses, mainly driven by *Herschel* open and guaranteed time surveys and their follow-ups. New techniques pioneered with *Herschel* are capable of detecting lenses in much higher numbers and to much higher redshifts than previous optical/near-IR surveys such as SLACS or SLQS (Bolton *et al.* 2006, Oguri *et al.* 2006). This paper will briefly review some recent key infrared lensing results with a particular focus on the multiwavelength spectral energy distributions and on new data from *Herschel*.

2. Galaxy cluster lenses

Some of the first images made public from *Herschel* were the SPIRE guaranteed time $250-350-500\,\mu$m images of the galaxy cluster lens Abell 2218. This well-known system

is one of several to have been used to constrain the 850 μm background population (e.g. Knudsen *et al.* 2008). Recently, Hopwood *et al.* (2010) had also used the Japanese *AKARI* facility to make its deepest 15 μm galaxy population constraints in this field, finding they could account for 87% of the predicted extragalactic background at this wavelength. At the time of writing, the SPIRE data in this cluster has not been published despite the data release, but Hopwood *et al.* (in prep.) have stacked the *AKARI* population in the submm maps and found that at least 41% (27%) of the background at 500 μm (250 μm) is attributable directly to the 15 μm population. At far-IR wavelengths, Altieri *et al.* (2010) presented *Herschel* guaranteed time PACS data of this cluster at $100 - 160\,\mu$m, demonstrating a constraint on the source counts comparable with that of the ultra-deep GOODS-North maps and accounting for $(55 \pm 24)\%$ and $(77 \pm 31)\%$ of the DIRBE direct measurements at 100 μm and 160 μm respectively. The prospects are clearly excellent for more extensive *Herschel* cluster lens work (e.g. Egami *et al.* 2010).

3. Field lenses: the promise of Herschel

3.1. *Proofs of concepts*

Gravitational lenses were originally hard to discover. For example, the Cosmic Lens All-Sky Survey (CLASS) observed nearly 12,000 flat-spectrum radio sources, finding 16 lenses (Myers *et al.* 2003). The large public SDSS database led to more rapid lens discovery (e.g. Bolton *et al.* 2006), though at low lens redshifts by virtue of the selection criteria.

The steep source counts in the submm imply a strong magnification bias. Prior to *Herschel*, the expectation was that about 50% of galaxies with 500 μm flux densities above $S_{500} > 100$ mJy would be lenses, with the remainder easily identifiable as local galaxies from optical imaging or as radio-loud AGN from radio data (Negrello *et al.* 2007). This prediction was supported by the mm-wave SPT counts. Spectacular confirmation came with the first *Herschel* candidates from H-ATLAS: in its first five lens candidates, Negrello *et al.* (2010) showed clear evidence of 2-image and 4-image lensing configurations from SMA data while Keck imaging showed only a foreground elliptical. There were therefore 5 lenses from first 5 candidates! The technique is much more sensitive to higher-redshift foreground lenses than SDSS-based selection and holds the promise of quickly and efficiently selecting large numbers of lenses.†

An associated breakthrough has been "blind" submm/mm-wave redshifts (e.g. Lupu *et al.* 2010, Frayer *et al.* 2011, Scott *et al.* 2011) with Z-spec (CSO) and Zpectrometer (GBT), with IRAM confirmations. This finally circumvents the torturous process of multi-stage multi-wavelength cross-IDs and exhaustive 8/10-m-class spectroscopic campaigns. For lensing systems, it provides rapid and unequivocal confirmation of a submm emitter background to the optical galaxy.

3.2. *Spectroscopic diagnostics*

The redshift determination of blind submm/mm-wave spectroscopy also makes follow-up far-IR and submm emission line diagnostics possible. SPIRE FTS observations of redshift $z = 3.0$ H-ATLAS lens ID 81 by Valtchanov *et al.* 2011 found first detection of 88 μm [OIII] line at $z > 0.05$. The high [OIII]/far-IR ratio and the limit on [OI]/[CII] suggests an AGN contributes ionizing radiation, as also suggested by the high radio/far-IR ratio. Cox *et al.* (2011) detect multiple CO transitions and [CII] in the $z = 4.3$ H-ATLAS galaxy SDP ID 141; their interpretation is of a PDR with a warm ($\simeq 40$ K) dense (10^4 cm^{-3})

† The *Herschel* lensing was also covered by the BBC series Bang Goes The Theory in September 2011, in which the Open University are co-producers and partners.

https://doi.org/10.1017/S1743921312009660 Published online by Cambridge University Press

gas, and the low line/far-IR ratio suggests again a high ionization parameter. Progress in detecting these diagnostics is fast: Lupu *et al.* 2011 present early results from high-density gas tracers in lensed submm galaxies, including HNC, HCN, HCO^+ and ^{13}CO.

Omont *et al.* 2011 detected an H_2O transition in the $z = 2.3$ H-ATLAS galaxy SDP ID 17, arguing against a PDR on the grounds that the luminosity ratio $L(H_2O\ 2_{02} - 1_{01})/L(CO\ (8-7)$ is comparable to that of Mrk 231. This, plus the fact that $L(H_2O\ 2_{02} - 1_{01})/L_{\rm far-IR}$ is greater than that of Mrk 231, suggests the presence of an AGN. Van der Werf *et al.* (2011) detected four rotational H_2O transitions in the $z = 3.9$ lensed quasar APM 08279+5255, inferring the presence of warm gas (105 ± 21 K). An immediate corollary of both detections is that ALMA will detect H_2O in many more submm lenses.

3.3. *Imaging diagnostics*

Early work on the SEDs of the submm lenses found the background sources are very difficult or impossible to detect in optical imaging, while *Spitzer* $3.6-4.5\,\mu$m data can be used to detect the background sources (Hopwood *et al.* 2011). The immediate corollary is that *there is a class of lenses that are missed entirely in optically-selected samples*. The first HST data on these lenses (Negrello *et al.* in prep.) finds the first submm-selected Einstein rings, and with the benefit of the prior from the HST imaging, faint features can now be discerned in the ground-based imaging. Submm galaxies are known to have a wide variety of colours and obscurations so one might expect many to be detectable by *Euclid* at least in its near-infrared channel. The *Herschel* samples will be a crucial training set for strong lens discovery in *Euclid*.

3.4. *The luminosity function and refined lens selection*

Lapi *et al.* 2011 derived the submm luminosity function (LF) of H-ATLAS galaxies at $z > 1$ using a far-IR/submm colour-based photometric redshift estimator, calibrated against redshift determinations from CO spectroscopy. Local spiral galaxies and lensed sources were eliminating by rejecting galaxies with optical IFs. The derived evolving LF agrees with the predictions of an updated version of the Granato *et al.* 2001 model.

The steepness of the bright-end slope of the submm LF, together with the submm K-corrections, are the underlying causes of the steepness of the submm source counts. However the steepness of the LF suggests a means to improve the efficiency of the lens selection, and to extend it to fainter submm fluxes: if one can select galaxies at the bright end of the *luminosity function* then they should be prone to magnification bias in a similar way to the bright submm source counts. To do this requires relaxing the constraint in the Lapi *et al.* 2011 analysis of rejecting galaxies with optical IDs. Instead, González-Nuevo *et al.* (2011) use a high-redshift selection of submm galaxies based on their far-IR/submm colours, then use VIKING near-IR data and search for optical/submm photometric inconsistencies. This approach has led to the discoveries of lens candidates fainter than the 100 mJy 500 μm flux threshold of Negrello *et al.* (2010). The source counts of their lens candidates agree with magnification bias predictions of the Lapi *et al.* 2011 luminosity functions. Extrapolating to the full H-ATLAS survey, the authors estimate an astonishing $> 10^3$ strong lenses can be reliably detected in H-ATLAS alone, several times more than from using a simple monochromatic submm flux cut.

4. Differential magnification: curse or blessing?

Gravitational lensing is purely geometrical and therefore wavelength-independent. None-theless, in any astrophysical lens the magnification varies with position in the source plane, so if the background source is extended with intrinsic colour gradients,

https://doi.org/10.1017/S1743921312009660 Published online by Cambridge University Press

then the lensed source may have colours different to the unlensed case. This differential magnification could have a very significant effect on broad-band SEDs as well as on emission line diagnostics. Many authors assume, implicitly or explicitly, that these differential effects can be neglected, but this assumption is often wholly unjustified. Serjeant (2011) makes a statistical assessment of differential magnification for various photometric and spectroscopic diagnostics, a range of source redshifts and a constant comoving density of lenses. Here, I present the special case of a lens redshift ($z_{\rm l} = 0.9$) and source redshift ($z_{\rm s} = 2.286$) identical to those in the lens system IRAS F10214+4724.

The model background source is based on the Cosmic Eyelash (Swinbank *et al.* 2010), QSO 1148+5251 (Walter *et al.* 2009) and Mrk 231 (Van der Werf *et al.* 2010). There are three continuum components: an AGN, a starburst and cirrus, with relative bolometric fractions of 0.3:0.5:0.2. The AGN has a torus SED from Nenkova *et al.* 2008 peaking in the mid-IR, modelled as a circular region with 0.1 kpc radius. The starburst region is concentrated in four identical 50 pc-radius GMCs as per the Cosmic Eyelash, with a starburst SED from Efstathiou *et al.* (2000). The cirrus is an extended ellipse with 2.5 kpc major axis, ellipticity of 0.4 and a cirrus SED from Efstathiou *et al.* (2000). There are also emission line regions: a cool CO region tracing the cirrus with clumps modelled in the LVG approximation with a kinetic temperature of 20 K, density $100\,{\rm cm}^{-3}$, CO column $10^{14}\,{\rm cm}^{-2}$ and an external background temperature of $2.73(1 + z_{\rm s})$ K; warm CO regions with 0.4 kpc radii centred on the GMCs, with LVG model temperatures of 45 K, densities $10^4\,{\rm cm}^{-3}$ and CO column $10^{18}\,{\rm cm}^{-2}$; a circular warm H_2O region with 120 pc radius and a cool H_2O region with major axis 1 kpc (both H_2O regions follow the precedent of Mrk 231); a circular [CII] emission region offset by 0.6 kpc from the AGN, with a radius of 0.75 kpc, following the precedent of QSO J1148+5251. The foreground lens is modelled as the sum of a de Vaucouleurs' profile and a Navarro-Frenk-White profile, both typical of the SLACS population. The simulation is conducted at a resolution of $0.001''$.

A clear result of these simulations is that the apparent bolometric fractions of strong lenses (magnification $\mu > 10$) depend very strongly on the selection wavelength. Fig. 1 shows the bolometric fractions for a simulated lensed galaxy selected at 60 μm and at 500 μm, while Fig. 2 (left) shows the AGN bolometric fraction for the lensed galaxies selected at these wavelengths. At this source redshift, 60 μm (observed-frame) is close to the peak of the AGN bolometric output, while observations at 500 μm predominantly sample the star-forming and cirrus components. Clearly the probability distribution of the AGN bolometric fraction depends very strongly on the selection wavelength, though some lens configurations are common to both wavelengths. The effect is much weaker for moderate-magnification systems ($2 < \mu < 5$); in these systems, the observed bolometric fractions *are* unbiased estimators of the underlying values.

Another striking result is that the warm and cool H_2O regions are also subject to differential magnification, at least in strongly-lensed systems (magnifications $\mu > 10$). Fig. 2 shows the relative magnification factors of the warm and cool H_2O emission line regions. These components contribute a similar flux in Mrk 231 for upper energy levels under 200 K, while the warm component dominates at higher temperatures. There is clearly a long tail in Fig. 2 in which the warm component is boosted relative to the cooler, more extended component. A similar tail is present in the H_2O *vs.* 500 μm magnifications, and in H_2O *vs.* GMCs. The presence of this tail provides an alternative explanation for the detection of H_2O ($2_{02} - 1_{11}$) in an H-ATLAS galaxy (Omont *et al.* 2011) because $\simeq 2/3$ of the flux of this line in Mrk 231 comes from the compact warm component. Having said that, at moderate magnifications ($2 < \mu < 5$) there are no appreciable differential magnification effects in the H_2O lines.

https://doi.org/10.1017/S1743921312009660 Published online by Cambridge University Press

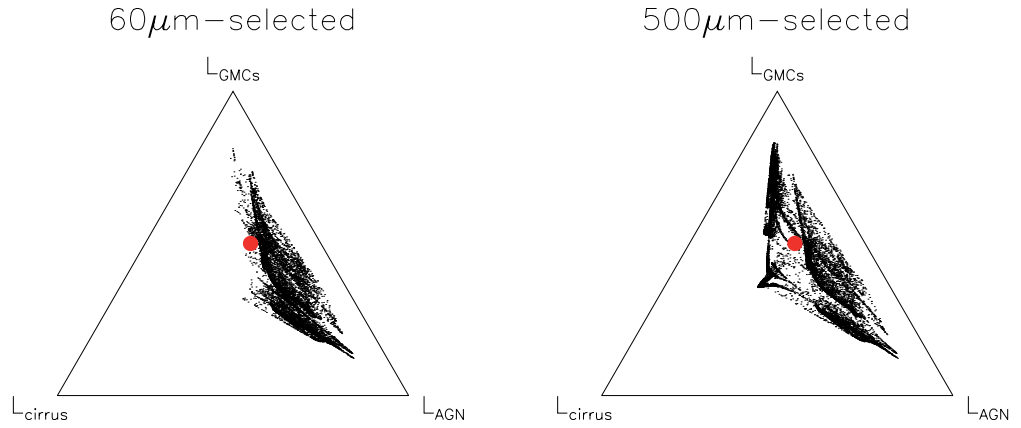

Figure 1. Bolometric fractions of strongly-lensed galaxies (magnifications $\mu > 10$, small dots, sparse-sampled for clarity) compared to the underlying background source fractions (large filled circle). These are ternary diagrams, i.e. the bolometric fraction is proportional to the perpendicular distance from an edge. At each apex, the bolometric fraction at that apex for that component is 100%, while the fraction is 0% at the opposite edge. Note the different distributions in 500 μm-selected and 60 μm-selected lenses.

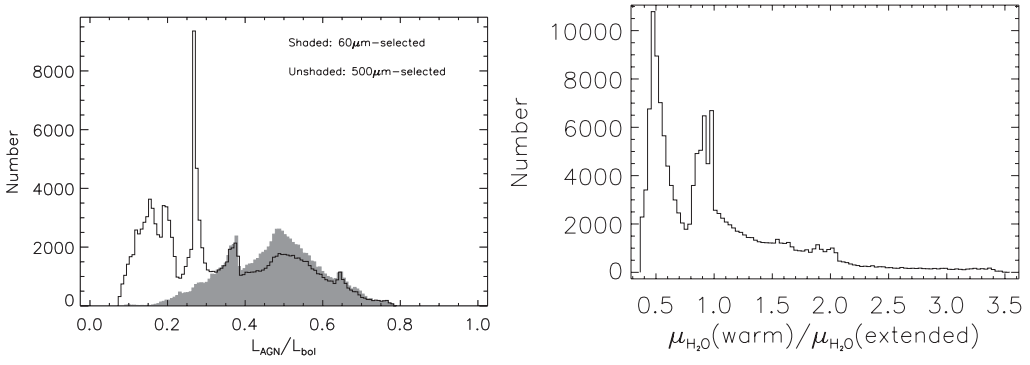

Figure 2. Left: AGN bolometric fractions in the simulated lensed galaxy, with monochromatic magnifications $\mu > 10$. Note that the probability distribution of bolometric fractions depends strongly on the selection wavelength. Right: relative magnification factors of the warm and cool H_2O lines discussed in the text, for a 500 μm-selected lenses with magnification $\mu > 10$.

Differential magnification also affects the observed bolometric fraction of the [CII] line (e.g. Valtchanov *et al.* 2011). However, in this case the bolometric fractions vary by $\simeq 0.1 - 0.2$ dex, comparable to the measurement uncertainties. Simulating the [CII] and CO line diagnostic diagram in Valtchanov *et al.* 2011 (not shown), it appears that the dynamic range of the diagnostic is much larger than that of the differential magnification effects, so this diagnostic is only weakly affected by differential lensing.

Finally, there is a serious distortion of the CO ladder. Fig 3 shows the predicted lensed CO Spectral Line Energy Distributions (SLEDs), compared to that of the underlying background source. This time, even moderate-magnification systems are affected. The warm CO is located very close to the GMCs in the model galaxy, but this does not necessarily guarantee that the warm CO is boosted relative to the cool component, even if selecting at 500 μm. Unlike the case of the [CII] and CO line diagnostic diagram in

https://doi.org/10.1017/S1743921312009660 Published online by Cambridge University Press

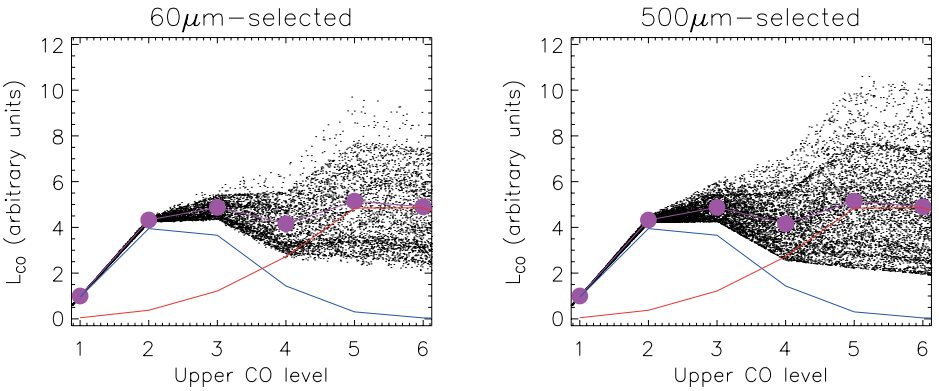

Figure 3. CO Spectral Line Energy Distribution (SLED) for the underlying source (large points), comprised of the warm and cool components (filled lines). Also shown as a shaded region is the range spanned by the differentially magnified simulated galaxies. Clearly, irrespective of selection wavelength, the CO SLED is strongly affected. This effect is more or less equally present for magnification $\mu > 10$ lenses (shown) and $2 < \mu < 5$ lenses.

Valtchanov *et al.* 2011, the useful dynamic range of the CO SLED is much smaller, making it much more sensitive to differential magnification effects.

Differential magnification is therefore a serious problem if its effects are not accounted for. Both the SED and emission line ratios are significantly distorted in galaxies with magnifications $\mu > 10$, and the CO SLED is very strongly distorted in any system with $\mu > 2$. However if a foreground mass model is available and the source is resolved, it can nevertheless work to our advantage. Lensing conserves surface brightness, so regions of high magnification are subject to angular magnification. This may, for example, provide uniquely high angular resolution views of active nuclei or star-forming regions in infrared-luminous galaxies. Observations by ALMA or eMerlin will easily detect lens morphologies, and an eMerlin legacy survey follow-up of submm-selected lenses is already underway.

These results are robust to changes in the assumed configuration of the background source. Only if the background source is broadly homogeneous could strong differential magnification effects be avoided. One might argue that the number of GMC regions could be much larger, e.g. to resemble those in $z = 0$ spiral discs (and at variance with observations of high-redshift infrared-luminous galaxies), but an active nucleus will inevitably create a colour gradient in the background source. Serjeant (2011) shows that the same effects are present for a constant comoving population of lenses, generalising the fixed lens redshift of $z_l = 0.9$ in this paper, and for different source redshifts.

5. Conclusions

Galaxy cluster lenses are a rapid route to probing the populations dominating the cosmic infrared backgrounds, both through direct detections and stacking analyses. The bulk of the observed or predicted cosmic infrared backgrounds at 15 μm, 100 μm, 160 μm and 850 μm have now been resolved into individual sources through ultra-deep imaging in the fields of foreground gravitationally-lensing galaxy clusters. Meanwhile, there is a clear need for larger numbers of strong galaxy-galaxy lens systems, particularly at higher lens redshifts. Following the spectacular confirmation of the $\sim 100\%$ gravitational lens selection efficiency from submm-selected lenses, there is now a tremendous scope for such lens discovery in the submm with *Herschel*. A further breakthrough has been "blind"

https://doi.org/10.1017/S1743921312009660 Published online by Cambridge University Press

submm/mm-wave redshift determination, i.e. without recourse to the torturous multi-stage multi-wavelength cross-identification and long-term 8m/10m-class optical/near-IR spectroscopy. Emission line diagnostics already yielding constraints on the physical conditions in these lensed galaxies. However, differential magnification effects cannot be neglected. In particular, the observed CO SLED in any lensed system can easily be un-representative of the SLED in the underlying source. Furthermore, the uncorrected bolometric fractions of strongly-lensed galaixes (magnifications $\mu > 10$) inferred from broad-band SEDs are so unreliable as to be useless.

SS thanks friends and colleagues the H-ATLAS (Eales *et al.* 2010) and HerMES consortia, whose results are quoted in this paper, STFC (grant ST/G002533/1) for financial support, and the conference organisers for the kind invitation.

References

Altieri, B., *et al.* 2010, *A&A*, 518, L17
Bolton, A. S., *et al.* 2006, *ApJ*, 638, 703
Cox, P., *et al.* 2011, *ApJ* in press (arXiv:1107.2924)
Eales, S. A., *et al.* 2010, *PASP*, 122, 499
Efstathiou, A., Rowan-Robinson, M., & Siebenmorgen, R. 2000, *MNRAS*, 313, 734
Egami, E., *et al.* 2010, *A&A*, 518, L12
Frayer, D. T., *et al.* 2011, *ApJL*, 726, 22
Gavazzi, R., *et al.* 2007, *ApJ*, 667, 176
Gavazzi, R., *et al.* 2008, *ApJ*, 677, 1046
González-Nuevo, J., *et al.* 2011, *ApJ*, submitted
Granato, G. L., *et al.* 2001, *MNRAS*, 324, 757
Hopwood, R., *et al.* 2010, *ApJL*, 728, 4
Hopwood, R., *et al.* 2011, *ApJL*, 728, 4
Knudsen, K. K., *et al.* 2008, *MNRAS*, 384, 1161
Lapi, A., *et al.* 2011, *ApJ*, in press (arXiv:1108.3911)
Lupu, R., *et al.* 2010, ApJ submitted (arXiv:1009.5983)
Lupu, R., *et al.* 2011, in The Molecular Universe, Proceedings of the 280th Symposium of the International Astronomical Union, Toledo, Spain, May 30-June 3, 2011
Myers, S. T., *et al.* 2003, *MNRAS*, 341, 1
Negrello, M., *et al.* 2007, *MNRAS*, 377, 1557
Negrello, M., *et al.* 2010, *Science*, 330, 800
Nenkova, M., Sirocky, M. M., Ivesić, Ž., & Elitzur, M. 2008, ApJ, 685, 147
Oguri, M., *et al.* 2006, *AJ*, 132, 999
Omont, A., *et al.* 2011, *A&A*, 530, L3O
Scott, K. S., *et al.* 2011, *ApJ*, 733, 29
Serjeant, S. 2011, *MNRAS* submitted
Smail, I., *et al.* 1997, *ApJL*, 490, L5
Swinbank, A. M., *et al.* 2010, *Nature*, 464, 733
Treu, T. 2010, *ARA&A*, 48, 87
Walter, F., *et al.* 2009, *Nature*, 457, 699
Valtchanov, I., *et al.* 2011, *MNRAS*, in press (arXiv:1105.3929)
Van der Werf, P. P., *et al.* 2010, *A&A*, 518, L42
Van der Werf, P. P., *et al.* 2011, *ApJ*, 741, L38